City Research Online

City St George's, University of London

Citation: Hada, S. L. & Rahman, B. M. A. (2019). Design of compact mode splitters using identical coupled waveguides with slots. OSA Continuum, 2(3), pp. 848-861. doi: 10.1364/osac.2.000848

This is the published version of the paper.

This version of the publication may differ from the final published version. To cite this item please consult the publisher's version.

Permanent repository link: https://openaccess.city.ac.uk/id/eprint/24862/

Link to published version: https://doi.org/10.1364/osac.2.000848

Copyright and Reuse: Copyright and Moral Rights remain with the author(s) and/or copyright holders. Copies of full items can be used for personal research or study, educational, or not-for-profit purposes without prior permission or charge, unless otherwise indicated, provided that the authors, title and full bibliographic details are credited, a hyperlink and/or URL is given for the original metadata page and the content is not changed in any way. For full details of reuse please refer to City Research Online policy.

City Research Online: http://openaccess.city.ac.uk/ publications@citystgeorges.ac.uk

Research Article Vol. 2, No. 3 / 15 March 2019 / OSA Continuum 848

Design of compact mode splitters using identical coupled waveguides with slots

S. L. HADA[1,*] AND B. M. A. RAHMAN[2]

[1]*Department of Electrical and Electronic Engineering, School of Engineering, Kathmandu University, Dhulikhel, Nepal*
[2]*Department of Electrical and Electronic Engineering, School of Engineering, City, University of London, London, EC1V 0HB, UK*
[*]*surendrahada@yahoo.com*

Abstract: In the past, multimode transmission through fibers has not been considered a preferred means of signal propagation due to the intermodal dispersion, which limits the data rate. However, recently, there has been an interest in using different modes as individual channels to increase the overall data rate. However, the challenging task in implementing such a system is that each individual mode has to be excited separately without mixing, and these should remain separated even at the bents and splices, and finally, they need to be collected separately. In this paper, design and optimization of a compact optical mode splitter by introducing a small slot in a silicon nanowire waveguide is demonstrated by employing a full-vectorial finite element method. The authors report here that by creating a slot within a waveguide, the desired coupling length ratio of 1:2 between the fundamental and the second modes can be obtained. The waveguide junctions have also been analyzed by using a rigorous least squares boundary residual method to study power transfer efficiency and effect of fabrication tolerances.

© 2019 Optical Society of America under the terms of the OSA Open Access Publishing Agreement

1. Introduction

The rapidly increasing demand for Internet bandwidth created a challenge to the network provider to cater for such bandwidth requirement and satisfy the transmission capacity by using single mode optical fiber. Therefore, there is an urgent need to develop and realise the novel concepts of multimode communication systems. One way to satisfy these demands is to consider space-division multiplexing, such as use of multicore fibers (MCFs) [1]. However, to use MCF in a transmission system does require stringent coupling technique to couple power in and out of each channel [2]. Furthermore, the performance of a MCF can be deteriorated due to the increased cross-talk resulted from the closely packed cores [3]. An alternative approach could be the adaptation of multiple-input multiple-output signal processing over multimode fibers (MMFs) [4]. In this case, mode selective couplers [5] or filters [6] can be used to excite different signal channels as different modes of a MMF and thus form independent data channels in a MMF [7]. However, generation of a specific mode in a MMF can also excite unexpected higher order modes, and this would degrade the transmission quality of the MMF [8]. In order to circumvent this problem, there is a requirement to excite the modes individually and thus to design components such as a mode splitter, which can separate different modes and so can treat them as independent transmission channels.

2. Theoretical background

Earlier, optical mode splitters to couple light from single mode to multimode [9] fibers and as a mode filter [10] have been reported. Mode splitter based on triple-core waveguide has also been reported in a two-mode fiber systems for mode selection and mode splitting [11]. Although a fiber based mode splitter may couple to optical fiber links better, however, often a compact photonic integrated circuit (PIC) based design can be considered to integrate such mode splitter

#357884 https://doi.org/10.1364/OSAC.2.000848
Journal © 2019 Received 17 Jan 2019; revised 24 Feb 2019; accepted 24 Feb 2019; published 12 Mar 2019

OSA CONTINUUM

with other functional devices. Silicon PIC with lower than 5 μm bending radius can yield a very compact functional device, however, to mitigate coupling loss various coupling approaches are being considered, such as grating couplers [12] and tapered [13] or uniform spot-size coupler [14] to couple silicon PIC to an optical fiber with a significantly larger spot-size. Such mode splitters can be designed by using asymmetrical Y-splitter [15], MMI [16] and micro-ring [17] based approaches. More recently mode splitters using asymmetrical directional couplers [18], and asymmetrical directional couplers incorporating slot waveguide in one branch [19] have been reported. However, the output power reduces rapidly with any change in the designed parameters. Although this is shown to improve by introducing a tapered asymmetrical coupler [20], the total output power can often reduce for tapered coupler.

Recently, our group has also shown [21] design optimisation of a mode splitter using an asymmetrical coupler. But, such coupler can be more sensitive to fabrication tolerances. In the work presented here, a novel concept of designing a compact mode splitter is proposed to separate higher order modes from the fundamental mode by using a symmetrical coupler. Since confinements of different modes are different, so their coupling lengths are also different. Therefore, we have considered to evaluate directional coupler as a possible mode splitter to separate different modes and treat them as individual transmission channels. Coupling length (L_c) of a directional coupler depends on different factors, such as, width (W) and height (H) of the waveguides and, also separation (S) between them. In this paper, since mode splitting is our main objective, optimization of the L_c ratio (L_R) for these modes, is considered first.

3. Results: directional coupler as a mode splitter

A full-vectorial Finite Element Method (FEM), based on the **H**-field formulation, is utilized to obtain the supermodes of coupled optical waveguides [22]. Since the mode splitting depends on their coupling length ratio, we identify the ratio between the fundamental mode and a given higher order mode as m:n, where m and n are required to be odd and even integer numbers, respectively or vice-versa. Thus, the key equation for calculating device length, L is,

$$L = m \cdot L_c^{11} = n \cdot L_c^{ij} \tag{1}$$

and L_R is the ratio of the coupling lengths for these two modes, as;

$$L_R = L_c^{11} / L_c^{ij} \tag{2}$$

where L_c^{11} and L_c^{ij} are the coupling lengths for the fundamental and a targeted higher order (ij^{th}) modes, respectively. This can be illustrated by a schematic diagram as given in Fig. 1. In this case, when m is odd, say 1, for the H_{11}^y mode, and n is even, say 2, for the H_{21}^y mode, the H_{11}^y will appear in the cross-port and H_{21}^y in the bar-port [23], as illustrated in Fig. 1.

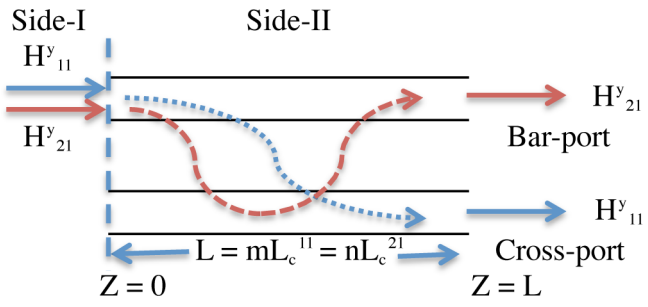

Fig. 1. Schematic Diagram of a Mode Splitter

OSA CONTINUUM

In this work, we have focused to achieve a specific coupling length ratio between the fundamental mode and a given higher order mode. However, it is also known that for any computational approach, the solution accuracy depends on the numerical parameters used. So, first, we focused on the effect of mesh variation as the FEM solution accuracy can critically depend on this parameter. Using the **H**-field based FEM, numerical simulation of Silicon nanowire waveguide directional coupler was performed considering different height and width of the guides and separation between them. Refractive indices of silicon core, silica buffer underneath and upper air cladding are taken as 3.47638, 1.44427 and 1.0, respectively at the operating wavelength of 1550 nm [24]. Figure 2 shows variations of the propagation constant, β, with the mesh division for even (β_e) and odd (β_o) H_{11}^y supermodes for a directional coupler with Width, W= 840 nm, Height, H= 300 nm, and Separation between two guides, S= 100 nm. Here, equal mesh divisions ($N_x = N_y$) in both the transverse directions are used. It can be observed that, initially β increases rapidly when the mesh is increased from 250×250 to 500×500 divisions. When mesh division is higher than 500×500, the incremental change in β is very small and reaches a saturation level beyond mesh 750×750. To test the convergence, a powerful approach, the Aitken's extrapolation method is also used, considering the 3 successive solutions of the β values obtained by employing a geometric mesh division ratio of 1:2:4. Following equation can be used to find the Aitken's extrapolated value [25]:

$$x_\infty = x_{r+1} - \frac{(x_{r+1} - x_r)^2}{x_{r+1} - 2x_r + x_{r-1}} \tag{3}$$

where, x_{r-1}, x_r, x_{r+1} are the results for three progressively increased mesh refinements, and x_∞, is the resulting extrapolated result. From these results, errors in the calculation of both the propagation constants were 0.0024% only, using Aitken's extrapolation with mesh division ratios of 250×250:500×500:1000×1000.

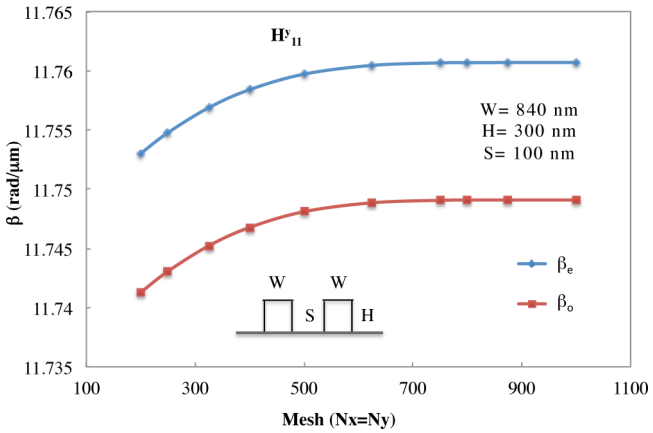

Fig. 2. Variations of the Propagation constant, β with the Mesh division

The coupling length, L_c, of a given mode can be calculated by using these β values as:

$$L_c = \frac{\pi}{\beta_e - \beta_o} \tag{4}$$

Variation of coupling length for the fundamental H_{11}^y mode, L_c^{11} with the mesh is shown in Fig. 3 by a solid blue line. As both β_e and β_o increases with the mesh, as shown in Fig. 2, their difference $\Delta\beta$, is more stable with the mesh variation. However, as L_c is inversely proportional to the $\Delta\beta$, so L_c variation can be very sensitive for weakly coupled waveguides as $\Delta\beta$ is smaller in these cases. Figure 3 shows initially, the coupling length, L_c^{11} increases with the mesh, after

OSA CONTINUUM

which it reaches a constant value. Although not shown here, same applies to the coupling length for the second H_{21}^{y} mode, L_c^{21} but as their convergences were different, the resulting L_R decreases slightly with the mesh and then becomes almost constant when $N_x = N_y \geq 750$. Using Eq. (3), its accuracy is again tested, and it was calculated that error for L_c^{11} was smaller than 0.00064%. However, error for L_c^{21} was slightly larger, about 0.0172% when 1000×1000 mesh divisions was used. From these two coupling lengths, L_c^{11} and L_c^{21}, their ratio, $L_R = L_c^{11}/L_c^{21}$, was calculated. Using again Aitken's extrapolation, it was determined that error in the ratio calculation was only 0.0068%.

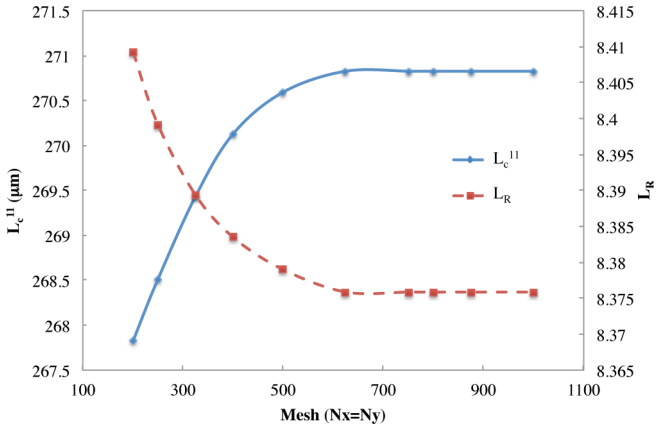

Fig. 3. Variations of L_c^{11} and L_R with the Mesh division

As it was observed that the typical accuracy in L_c values and their ratio are adequate when a mesh division 750×750 or higher is used, so subsequently, 750×750 mesh has been used for all the numerical simulations. In these cases, more than 1 million first order triangles are used to represent only half of the directional coupler cross-section (as symmetry conditions of the directional coupler was also exploited). In this case, the resulting horizontal and vertical mesh sizes inside the waveguide core are better than 2 nm and 1 nm, respectively.

We have carried out numerical simulations of typical silicon waveguide couplers for a range of combinations of different waveguide width (650 to 1015 nm), height (250 to 500 nm), and separation between them (100 to 200 nm).

With the standard directional coupler, for the various physical dimensions we have considered, the L_R was found to be varying between 6 to 10. Variations of the L_R with the separation between the waveguides for two different widths are shown in Fig. 4. In this case, the core height was 300 nm. It can be observed from this figure that for W= 750 nm, when S= 125 nm, the L_R is close to 10. Although this satisfies the design requirement, given in Eq. (1), but being m=1 and n=10, such a higher ratio, L_R= 10, would make the device not only very long, but also performance will become more sensitive to the fabrication tolerances. It can be observed that wider W may reduce the L_R slightly but associated longer coupling length not only makes the device much longer but also weak coupling makes the device more sensitive to the fabrication tolerances. It can also be noted here that for the increase in waveguide separation, the L_R also increases.

Variation of L_R with the waveguide height, H for two different widths, 1000 nm and 900 nm are shown in Fig. 5 by a dashed red line and a solid blue line, respectively. In this case, separation between the waveguides, S, was kept constant at 100 nm. It can be observed that, as the waveguide height, H, is increased the L_R is reduced. The lowest L_R in this case was found to be 6. Moreover, with the increase in waveguide width, L_R also reduces, as shown in Fig. 5. It can also be observed that L_c^{21} increases when the waveguide height increases as shown here

OSA CONTINUUM

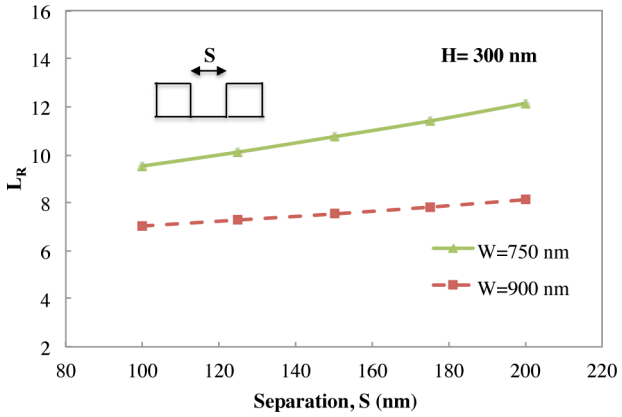

Fig. 4. L_R variation with the Separation (S)

by a green line, as for a larger waveguide, modes are more confined. It can be observed here that although for larger H and W, the L_R ratio can be reduced slightly but the resulting coupling length and the splitter length would be excessively large in these cases.

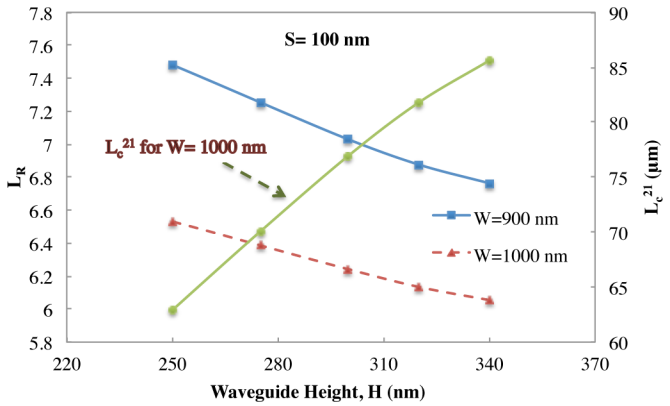

Fig. 5. L_R and L_c^{21} variation with the Height for the H_{21}^y Mode

During the course of numerical simulations, we have identified three quasi-TE and three quasi-TM guided modes, when the waveguide width is 850 nm with its height 300 nm. Amongst these modes, the separation between the modal indices of the H_{21}^y and H_{11}^x mode is the smallest and this can cause mode degeneration and polarization conversion particularly when the waveguide width varies between 810 nm and 870 nm.

4. Modification of the directional coupler

We have observed that by changing the separation, width and height of typical coupled nanowire waveguides, it would not be possible to achieve a satisfactory design, since in all the cases, the m:n ratio was very high. Our objective has been to design a mode splitter, using a symmetric coupler, which can also yield a compact design with a smaller L_R value between the fundamental and higher order modes.

In this paper, we report a novel concept by introducing a slot in the middle of a nanowire waveguide, which strongly influences modal properties of the fundamental (H_{11}^y) mode but very

OSA CONTINUUM

small effect on the second mode, H^y_{21}. The schematic cross-section of the proposed structure is shown in Fig. 6, where, W is the waveguide width, H is the waveguide height, S is the separation between the waveguides, t is the slot-height and δ is the slot-width.

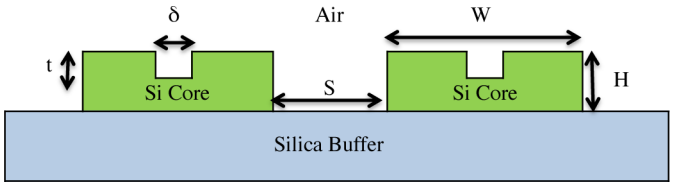

Fig. 6. Cross-section of a modified Symmetrical Directional Coupler

The effect of slot in a waveguide can be explained by observing the variation of the dominant H_y field along the x-direction. Variations of the dominant H_y field of the H^y_{11} even supermode along the horizontal x-direction are shown in Fig. 7 (a). In this case, vertical position was selected in the middle of the silicon bridge, below the slot. The H_y field profile for the waveguide without the slot is shown by a solid blue line. This shows the peak value of the H_y field is at the center of the waveguide. The H_y field profile for the waveguide with the slot is shown here by a dashed red line. It can be seen that due to the presence of the slot, the H^y_{11} field is affected, illustrated by a dip near the slot region. Similarly, dominant H_y field profile of the H^y_{21} mode along the x-axis, with and without a slot are shown in Fig. 7 (b), by a dashed red line and a solid blue line, respectively. It can thus be observed that the presence of a slot has a negligible effect on the H^y_{21} mode, since near the slot, field was close to zero. Hence, it can be expected that the coupling length for the H^y_{11} mode will reduce since its modal confinement was also reduced, while that of the H^y_{21} mode will remain almost unaffected. Thus, L_R is expected to reduce significantly, as the coupling length of H^y_{11} mode would reduce drastically, while that of the H^y_{21} mode will remain similar.

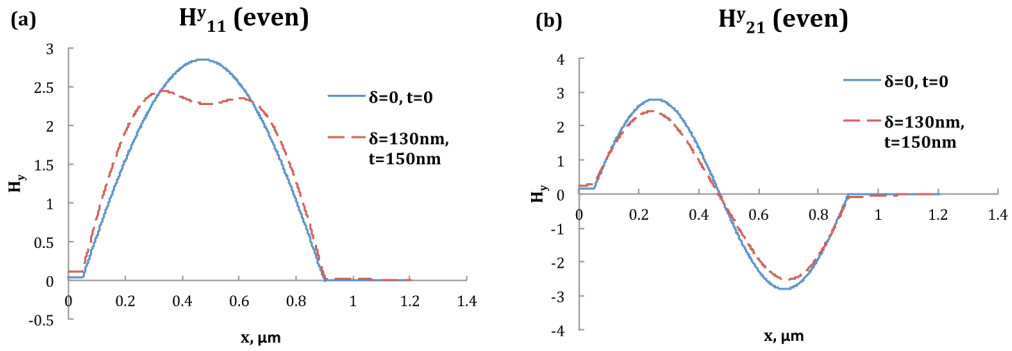

Fig. 7. H_y field variation along the x-direction: (a) H^y_{11} even Supermode; (b) H^y_{21} even Supermode

With this modified structure, it may be possible to achieve the desired coupling length ratio by varying W, H, S, δ, and t. Numerical simulations were carried out with constant H= 300 nm and S= 100 nm, but for different δ and t. Figure 8 shows the variations of L_R with t, for W= 850 nm and 950 nm by a solid green line and a dashed blue line, respectively, for a fixed δ = 150 nm. It can be clearly observed that the L_R reduces with the increase of slot-height, t. In this case, the ideal L_R of '2' can also be achieved in two different slot-heights at 143 nm and 182 nm for W= 850 nm and 950 nm, respectively.

OSA CONTINUUM

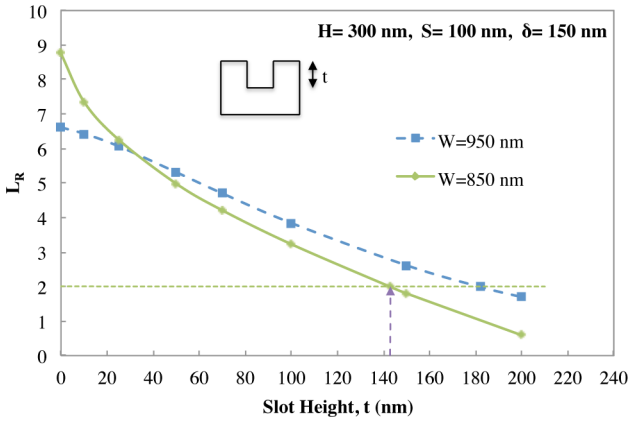

Fig. 8. Variation of L_R with the Slot-height (t)

Figure 9 illustrates the variation of L_R with the slot-width, δ for W= 850 nm and 950 nm by a solid green line and a dashed blue line, respectively, when t was fixed at 150 nm. It can be observed that it is also feasible to achieve ideal L_R value of '2' by adjusting these parameters, and this can be obtained at δ= 130 nm, as shown in Fig. 9. The L_c^{11} value at this point is 108.82 μm and L_c^{21} is 54.26 μm. Thus, at the end of a 108.82 μm long directional coupler section, H_{11}^y mode will exit through the cross-port, whereas, H_{21}^y mode will come out of the bar-port. It can also be observed from this figure that for a small change in the slot-width, the resulting L_R value is reasonably stable.

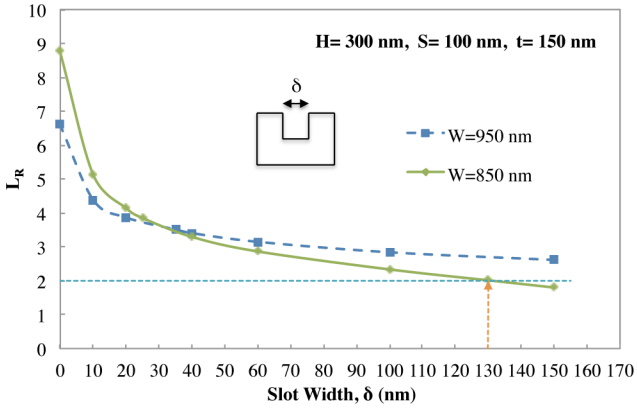

Fig. 9. Variation of L_R with the Slot-width (δ)

From Fig. 9, it can also be observed that it is impossible to achieve the ideal L_R value of '2' for W= 950 nm, as shown by the dashed blue line. However, it was shown in Fig. 7 (a) that the mode profile in a coupled Silicon nanowire waveguide is no longer perfectly symmetric along the vertical center of an individual waveguide. So, it is expected that exploiting the field asymmetry, a slight asymmetrical placement of the slot might improve the optimisation of the mode splitter. So next, position of the slot is shifted a bit, by introducing Δx shift outwardly from the center, as shown in the inset of Fig. 10. As expected, it is shown in Fig. 10 that the L_R clearly reduced to '2' for the same W, H, S, δ and t when 'Δx' is positive (shifting outwards) by 11 nm, which was not possible in this case without an offset.

OSA CONTINUUM

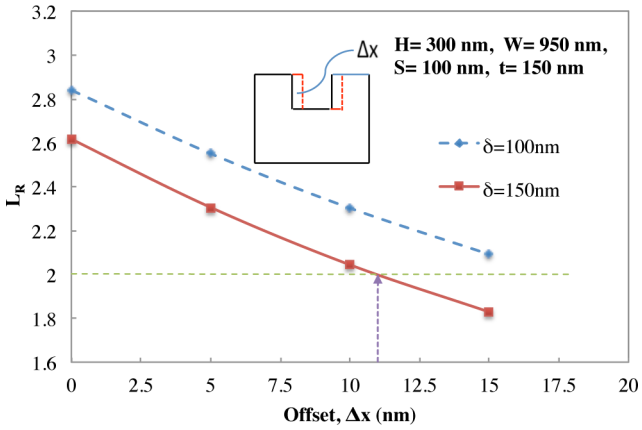

Fig. 10. L_R Variation with the Offset of Slot-width Position (Δx)

The above results suggest that by adjusting height and width of the waveguide along with the slot-height and slot-width, it would be possible to design a compact and more realistic mode splitter. If needed, the position of the slot within the waveguide can also be adjusted to achieve the desired L_R. However, to consider the best design, we also need to analyse its power loss and supermode coupling coefficients at the junction and this is carried out by using the full-vectorial least-squares boundary residual (LSBR) method [26].

5. Power transfer calculation

The mode splitter consist of one input guide butt-coupled to a directional coupler and at the end of the directional coupler section two output ports are separated to stop further power coupling process. In order to characterise such waveguide discontinuities at the junction, a powerful numerical approach, the LSBR method [26] is utilized here, which rigorously imposes the continuity of the tangential electric and magnetic fields at the junction interface. The LSBR method looks for a stationary solution to satisfy these boundary conditions by minimizing the error energy functional, J, as given by [26],

$$J = \int_{\Omega} |E_t^I - E_t^{II}|^2 + \alpha \cdot Z_0^2 |H_t^I - H_t^{II}|^2 \, \mathrm{d}\Omega \tag{5}$$

where α is the dimensionless weighting factor to balance the magnetic and electric components of the error functional J, and Z_0 is the free-space impedance. Using this approach, insertion loss, coupled power, and cross-talk are calculated for different mode splitter designs.

6. Results: power transfer

To calculate the power transfer from input guide, Side-I, to the coupler section of the mode splitter, Side-II, and to find the losses suffered at the waveguide junction, an optimised design is considered with W= 850 nm, H= 300 nm, S= 100 nm, δ= 130 nm, and t= 150 nm, which yields L_R= 2 at the operating wavelength of 1550 nm. The LSBR method is used here to find the modal coefficients (also, known as scattering matrix at this junction, Z = 0+). In this case, the transmission coefficients for the H_{11}^y even and odd supermodes are found to be 0.705 and 0.703, respectively. Superposition of them will produce a field almost similar to the input H_{11}^y mode profile of the incoming waveguide to satisfy the continuity conditions. Similarly, the transmission coefficients for the H_{21}^y even and odd supermodes are found to be 0.697 and 0.684, respectively, when H_{21}^y mode is the incident field. From these values, it was calculated that the insertion loss,

OSA CONTINUUM

when an input isolated guide butt-coupled to the directional coupler section, for this design is only 0.0154 dB for the H_{11}^y mode and 0.045 dB for the H_{21}^y mode. At a distance L = L_c^{11} = 108.82 μm, these two even and odd H_{11}^y supermodes will be out of phase and their superposition will yield the H_{11}^y mode in the adjacent guide (cross-port). From these supermode coefficients and their modal field profiles we have calculated 98.24% power will be transferred to the cross-port. Only a small power will remain in the bar-port, and this cross-talk has been calculated to be -27.3 dB. Likewise, at the same distance L = $2L_c^{21}$ = 108.82 μm, as the total phase shift will be 2π, power will return to the original guide or the bar-port and this value is found to be 96.58% for the H_{21}^y mode, with a cross-talk (power remaining in cross-port) of −16.2 dB.

Next, dimension of slot-width is varied by ±10 nm, keeping other parameters same as before, in order to analyse the effect of fabrication tolerances. When, δ reduced to 120 nm, L_c^{11} increased by 2% to 111 μm and L_c^{21} decreased by 3.3% to 52.6 μm, thereby increasing the L_R to 2.11. In this situation, the insertion loss at the junction is found to be almost unchanged, 0.0163 dB for H_{11}^y mode and 0.042 dB for H_{21}^y mode. However, due to slight mismatch of the device length with their coupling lengths, the power coupled to the cross-port for H_{11}^y mode is found to be 98.3% but the power returned to the bar-port for H_{21}^y mode is reduced to 95.6%.

Again, when δ increased to 140 nm, L_c^{11} is reduced to 106.9 μm but L_c^{21} is increased to 56.25 μm, thereby reducing the L_R to 1.9. In this case, the insertion loss is found to be 0.0143 dB for H_{11}^y mode and 0.047 dB for H_{21}^y mode. However, power coupled from guide-I to guide-II for H_{11}^y mode is obtained as 98% and the power returned to the guide-I for H_{21}^y mode is found to be 95.4%. This analysis shows that with the increase in slot-width, L_R decreases, insertion loss and power coupled to cross-port decreases for H_{11}^y mode. But, in such case, insertion loss slightly increases for H_{21}^y mode and the power coupled to bar-port reduces when $\delta \neq$130 nm. These results are summarised in Table 1.

Table 1. Insertion loss, Power Coupled and Cross-talk with δ-variation for the H_{11}^y and H_{21}^y modes

Slot-width	Insertion Loss (dB)		Power Coupled (%)		L_c Ratio	Cross-talk (dB)	
δ	H_{11}^y	H_{21}^y	H_{11}^y	H_{21}^y	L_R	H_{11}^y	H_{21}^y
120	0.0163	0.042	98.30	95.60	2.11	−25.6	−14.7
130	0.0154	0.045	98.24	96.58	2.0	−27.3	−16.2
140	0.0143	0.047	98.0	95.40	1.9	−25.6	−14.6

Variations of coupled power with the slot-width, δ, are shown in Fig. 11. It can be observed that power coupling varies between -0.06% to 0.24% for the H_{11}^y mode and 1.01% to 1.22% for the H_{21}^y mode from the original power coupling values, as shown by the solid blue line and dashed red line, respectively. The power coupling variation is slightly higher for the H_{21}^y mode, which is due to the fact that not only % change of L_c^{21} was higher, but also any phase error due to coupling length variation doubles, as n= 2 for the H_{21}^y mode, compared to m= 1 for the H_{11}^y mode. So, H_{21}^y mode is more sensitive to any changes in its coupling length. However, insertion loss variation is very small for both the modes. Cross-talk values are also shown in Table 1, which shows only a small change with the slot-width variation.

Next, effect of change in the slot-height, t, on the device performance is studied. In case of the slot-height, it is varied by ±10 nm from the original design value of 150 nm. When t reduced to 140 nm, L_c^{11} increases by 10.3% to 120 μm and L_c^{21} reduces slightly by 1.9% to 53.23 μm, resulting in a L_R of 2.25. The insertion loss, so far, is found to be almost unchanged for both the H_{11}^y and H_{21}^y modes, as shown in Table 2. In this case, power coupled to adjacent guide-II (cross-port) for H_{11}^y mode is 96.4% and power returned to guide-I (bar-port) for the H_{21}^y mode is 96.7%. Similarly, when t increased to 160 nm, L_c^{11} decreases by 9.7% to 98.26 μm and L_c^{21} increases by 2.2% to 55.45 μm, resulting in a L_R of 1.77. Insertion losses in this case are also

OSA CONTINUUM

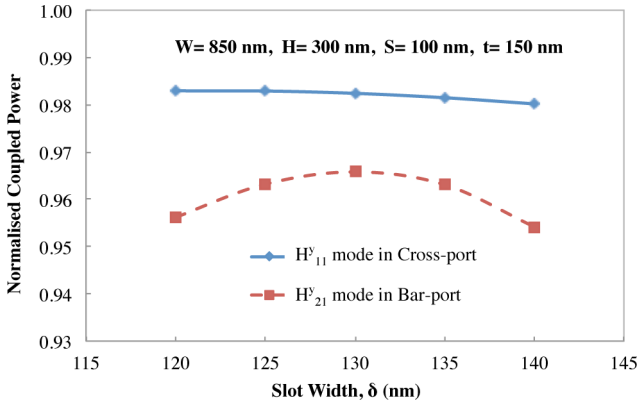

Fig. 11. Variation of Coupled Power with the Slot-width (δ)

almost same for both the modes, as shown in Table 2. Likewise, 95.2% power of the H_{11}^{y} mode is coupled to the cross-port and 95.6% power of the H_{21}^{y} mode is coupled to the bar-port. All these results including the cross-talk values are shown in Table 2.

Table 2. Insertion loss, Power Coupled and Cross-talk with *t*-variation for the H_{11}^{y} and H_{21}^{y} modes

Slot-height	Insertion Loss (dB)		Power Coupled (%)		L_c Ratio	Cross-talk (dB)	
t	H_{11}^{y}	H_{21}^{y}	H_{11}^{y}	H_{21}^{y}	L_R	H_{11}^{y}	H_{21}^{y}
140	0.0155	0.032	96.40	96.70	2.25	−16.6	−15.8
150	0.0154	0.045	98.24	96.58	2.0	−27.3	−16.2
160	0.015	0.062	95.20	95.60	1.77	−15.2	−15.2

With the variation of the slot-height, H_{11}^{y} mode seems less affected, whereas, for H_{21}^{y} mode, the results for insertion loss and power coupled is slightly better when t is reduced. It can be observed that for a deviation from the original design by ±10 nm changes in slot-height the insertion loss is found to change between −0.003% to 0.008% for the H_{11}^{y} mode and −0.31% to 0.4% for the H_{21}^{y} mode. The coupled power varies between 1.87% to 3.09% for the H_{11}^{y} mode and -0.12% to 1.01% for the H_{21}^{y} mode. It should be noted that Insertion loss is less affected by the change in slot-width or slot-height. However, changes in the power coupled to the appropriate port changes more with the variation in the slot-width and slot-height due to the accompanied change in both L_c and L_R, which introduces mismatch between the device length with the changing coupling lengths.

Based on the above results for δ and t variation, it can be inferred that for power transfer efficiency, δ variation influences the mode field of H_{11}^{y} mode, as it affected its coupling length, whereas, t variation affects the mode field of H_{21}^{y} mode because of larger phase error associated with n being equal to 2. Thus, it is necessary to choose the optimum value of δ and t, where both the modes are less affected. From Tables 1 and 2, it can be noted that the value of δ and t, which yields L_R of '2' is the optimum dimension of the slot for a given set of W, H, S, and λ and can be considered best design for a compact mode splitter, as the design is very stable related to any variation in the slot-width or slot-height during its fabrication.

Variations of coupled power with the waveguide width to two output ports are shown in Fig. 12. In this case, the H_{11}^{y} mode input power coupled to cross-port varies between 0.24% to 0.1% at the cross-port for ±10 nm change in the width, which is negligible. However, for the H_{21}^{y} mode, power transfer variation to bar-port was larger, reduced to 78.9% and to 91.06% for W= 840 nm and W= 860 nm, respectively. With the change in waveguide height from original design,

power transfer for H_{21}^{y} mode was worse, but however, it should be noted that typically fabrication accuracy in the waveguide height is often less than 5 nm, which is significantly better than its control in the width.

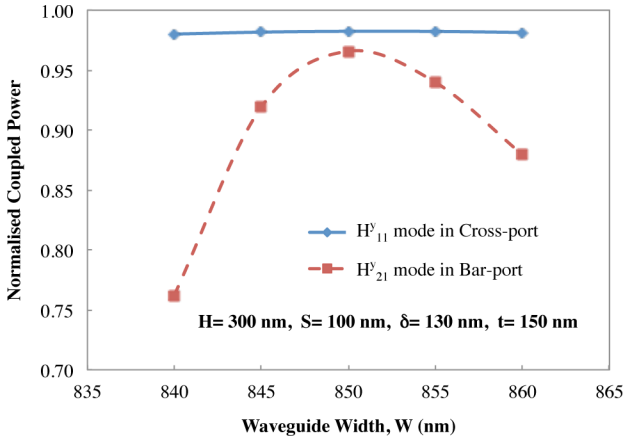

Fig. 12. Variation of Coupled Power with Waveguide Width (W)

Thermal tuning exploiting the large temperature dependent refractive index of silicon has been widely used to compensate the fabrication tolerances of silicon photonic devices [27]. Carrier dependent refractive index change has also been exploited in the design of silicon modulators and this approach has also been used for active compensation and to reconfigure micro-ring resonators [28]. However, these approaches consumes continuous additional power. Post-fabrication permanent trimming by exploiting oxide compaction [29], silicon oxidation [30], ion implantation [31] and photo-induced in chalcogenide clad [32] silicon devices have also been considered.

Variations of the coupled power at the desired ports with the separation between the waveguides are shown in Fig. 13. In this case, the percentage change in power coupled to the respective waveguides at Side-II for ±10 nm change in separation is found to be varied between 5.39% to 3.32% for H_{11}^{y} mode and 13.2% to 6.6% for H_{21}^{y} mode. It can be noted that coupled power variation is more when the separation is reduced from its original designed value for the H_{21}^{y} mode, similar to the cases for the variation with the waveguide width, or its height.

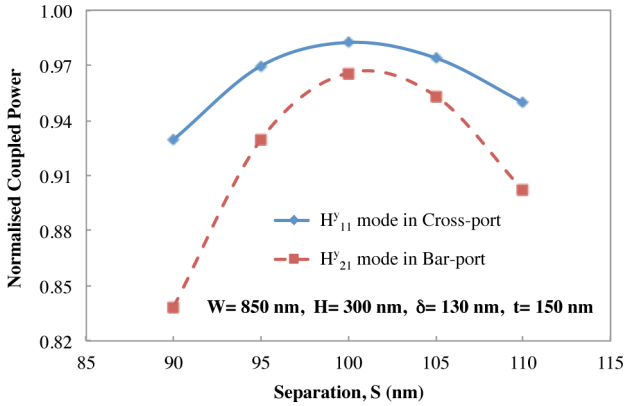

Fig. 13. Variation of Coupled Power with Separation (S)

OSA CONTINUUM

Finally, effect of the operating wavelength on the device performance is also studied and this is shown in Fig. 14. Variations of the normalised coupled power for the H^y_{11} mode and the H^y_{21} mode in cross and bar-ports are shown by a solid blue line and a dashed red line, respectively. It can also be seen that the coupled power variation for ±75 nm changes in operating wavelength, λ, stands between 5.95% to 8.06% and 26.6% to 28.8%, for H^y_{11} mode and H^y_{21} mode, respectively. However, operating between 1530 nm to 1565 nm, along the whole conventional C-band, H^y_{11} coupled power reduces by less than 0.6% and that of the H^y_{21} mode, by less than 2%.

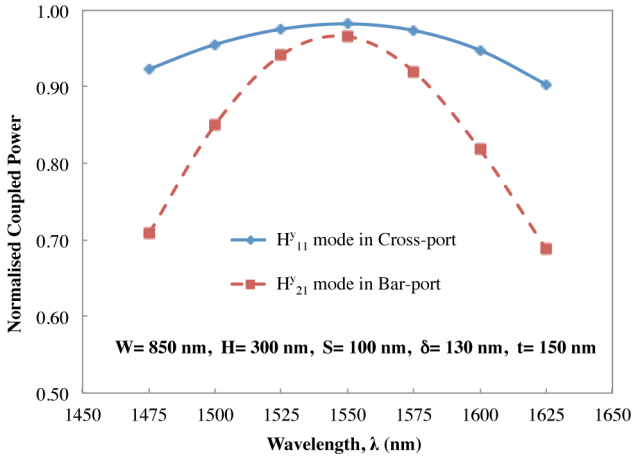

Fig. 14. Variation of Coupled Power with Wavelength (λ)

Thus, from the above figures, it is being observed that the fabrication tolerance is more critical with H^y_{21} mode, compared to that of H^y_{11} mode for variation with W, H, S, and λ. However, with δ and t, such variations were very small for both the modes. Again, the desired mode splitter ratio of 1:2 can be achieved by varying slot-width and slot-height. It should be noted here, as the design incorporates symmetrical coupled guides, these have better fabrication tolerances than those design incorporating non-identical coupler [21]. Therefore, the mode splitter design is more viable, if the parameters, such as, W, H, and S can be set at a certain values to make a design compact and the mode splitter ratio is fixed by varying δ and t only. In the above examples, it has been assumed that the input guide, also, have similar slots as required in the directional coupler section. However, in reality the input guide may be a standard Silicon guide without a slot. In this case, the insertion loss at the first junction would increase due to the mismatch between the waveguides. With the input guide as a standard waveguide and the slot waveguides at the Side-II, the LSBR result shows, insertion loss as 0.7806 dB for H^y_{11} mode and 2.5823 dB for H^y_{21} mode. Similarly, for the same combination, power coupled to cross-port is found to be 81.8% for H^y_{11} mode and to bar-port is 53.16% for the H^y_{21} mode. This shows loss is more when we use different waveguides at the Side-I and Side-II of the waveguide junction. However, it would be perfectly feasible to use a horizontally tapered slot to reduce the insertion loss and adiabatically reduction of the slot-width can be easily fabricated by using the standard CMOS technology.

7. Conclusion

For the first time, design of a novel mode splitter to separate fundamental mode from higher order modes for a multimode optical communication system is reported here, where individual mode can act as separate signal channel. Various design parameters, such as insertion loss, mode coupling and cross-talk, are rigorously simulated by using full-vectorial approaches. Although, effect of asymmetrical shift of slot has not been shown here, but we have estimated that for ± 5

OSA CONTINUUM

nm shift the coupling length change is below 10% and additional power loss would be less than 4%.

It has also been noticed that power coupling variation is higher in case of the H_{21}^{y} mode, compared to that of the H_{11}^{y} mode with the variation in W, H, S, and λ. However, such variations are negligible in case of changes in slot-width or slot-height, which can be considered as the major strength of this compact design, as it would be possible to split the modes efficiently by achieving m:n ratio as 1:2, the minimum ratio desired. This design presented here is similar to a silicon slot waveguide [33], with it's unique feature of guiding the light in a low index region allowing better light-matter interactions. Fabrication of such silicon slot waveguide with slot-width less than 100 nm and silicon core width smaller than 250 nm are routinely undertaken. It is expected that mode splitter presented here with slot-width 150 nm and silicon core width more than 350 nm would be similarly feasible. The overall system would also include bent sections to link various guided-wave sections. The coupling during the transient sections will be less than 0.01% [34]. Similarly, bending loss in silicon waveguides is very small. The bending loss for a larger nanowire with 850 nm wide, 300 nm high and 3 μm bending radius is only 0.0014 dB/cm, and this gives a 5 μm long 90 degrees bent section with total loss only 7×10^{-7} dB. In this paper, design optimization of a compact mode splitter is presented, which can be easily fabricated by using the standard CMOS technology, and this will facilitate to meet the increasing demands for the higher data rate requirements of the current telecommunications systems. Similarly, this concept can also be considered to split other higher order modes, by selecting multiple slots at locations of field maxima or zero value depending on the specific design requirement.

References

1. L. Yuan, Z. Liu, and J. Yang, "Coupling characteristics between single-core fiber and multicore fiber," Opt. Lett. **31**(22), 3237–3239 (2006).
2. B. Zhu, T. F. Taunay, M. F. Yan, M. Fishteyn, G. Oulundsen, and D. Vaidya, "70-Gb/s multicore multimode fiber transmissions for optical data links," IEEE Photon. Technol. Lett. **22**(22), 1647–1649 (2010).
3. J. M. Fini, B. Zhu, T. F. Taunay, and M. F. Yan, "Statistics of crosstalk in bent multicore fibers," Opt. Express **18**(14), 15122–15129 (2010).
4. A. Tarighat, R. C. Hsu, A. Shah, A. H. Sayed, and B. Jalali, "Fundamentals and challenges of optical multiple-input multiple-output multimode fiber links," IEEE Commun. Mag. **45**(5), 57–63 (2007).
5. B. Jalali, R. C. Hsu, and A. R. Shah, "Coherent Optical MIMO," in *Defense and Security*, International Society for Optics and Photonics, pp. 121–127, 2005.
6. C. Tsekrekos and A. Koonen, "Mode-selective spatial filtering for increased robustness in a mode group diversity multiplexing link," Opt. Lett. **32**(9), 1041–1043 (2007).
7. C.-p. Yu, J.-h. Liou, Y.-j. Chiu, and H. Taga, "Mode multiplexer for multimode transmission in multimode fibers," Opt. Express **19**(13), 12673–12678 (2011).
8. D. Sim, Y. Takushima, and Y. Chung, "High-speed multimode fiber transmission by using mode-field matched center-launching technique," J. Lightwave Technol. **27**(8), 1018–1026 (2009).
9. M. Fujiwara, K.-I. Suzuki, M. Oguma, S. Soma, and N. Yoshimoto, "High-splitting-ratio PON systems using a PLC-based funnel-shaped waveguide with dual-mode fiber," J. Opt. Commun. Netw. **7**(1), A1–A6 (2015).
10. Z. Lambak, K. Khairi, Z. Hamzah, and K. H. Fong, "Evaluation of mode filter in optical splitter by using method of lines," in *RF and Microwave Conference (RFM), 2011 IEEE International*, pp. 307–310, IEEE, 2011.
11. Z. Wang, Y. Wang, Y. Li, and C. Wu, "Mode splitter based on triple-core waveguide," Opt. Express **14**(22), 10324–10331 (2006).
12. T.-H. Loh, Q. Wang, J. Zhu, K.-T. Ng, Y.-C. Lai, Y. Huang, and S.-T. Ho, "Ultra-compact multilayer Si/SiO_2 GRIN lens mode-size converter for coupling single-mode fiber to Si-wire waveguide," Opt. Express **18**(21), 21519–21533 (2010).
13. L. Jia, H. Zhou, T.-Y. Liow, J. Song, Y. Huang, X. Tu, X. Luo, C. Li, Q. Fang, M. Yu, and G. Lo, "Analysis of the polarization rotation effect in the inversely tapered spot size converter," Opt. Express **23**(21), 27776–27785 (2015).
14. W. Jiang, N. Kohli, X. Sun, and B. M. A. Rahman, "Multi-poly-silicon-layer-based spot-size converter for efficient coupling between silicon waveguide and standard single-mode fiber," IEEE Photon. J. **8**(3), 1–12 (2016).
15. J. B. Driscoll, R. R. Grote, B. Souhan, J. I. Dadap, M. Lu, and R. M. Osgood, "Asymmetric Y junctions in silicon waveguides for on-chip mode-division multiplexing," Opt. Lett. **38**(11), 1854–1856 (2013).
16. T. Uematsu, Y. Ishizaka, Y. Kawaguchi, K. Saitoh, and M. Koshiba, "Design of a compact two-mode multi/demultiplexer consisting of multimode interference waveguides and a wavelength- insensitive phase shifter for mode-division multiplexing transmission," J. Lightwave Technol. **30**(15), 2421–2426 (2012).

OSA CONTINUUM

17. B. A. Dorin and N. Y. Winnie, "Two-mode division multiplexing in a silicon-on-insulator ring resonator," Opt. Express **22**(4), 4547–4558 (2014).
18. D. Dai, J. Wang, and Y. Shi, "Silicon mode (de) multiplexer enabling high capacity photonic networks-on-chip with a single-wavelength-carrier light," Opt. Lett. **38**(9), 1422–1424 (2013).
19. J. Liao, L. Zhang, M. Liu, L. Wang, W. Wang, G. Wang, C. Ruan, W. Zhao, and W. Zhang, "Mode splitter without changing the mode order in SOI waveguide," IEEE Photon. Technol. Lett. **28**(22), 2597–2600 (2016).
20. Y. Ding, J. Xu, F. Da Ros, B. Huang, H. Ou, and C. Peucheret, "On-chip two-mode division multiplexing using tapered directional coupler-based mode multiplexer and demultiplexer," Opt. Express **21**(8), 10376–10382 (2013).
21. C. Pan and B. M. A. Rahman, "Accurate analysis of the mode (de) multiplexer using asymmetric directional coupler," J. Lightwave Technol. **34**(9), 2288–2296 (2016).
22. B. M. A. Rahman and J. B. Davies, "Finite-element solution of integrated optical waveguides," J. Lightwave Technol. **2**(5), 682–688 (1984).
23. S. L. Hada and B. M. A. Rahman, "Design concepts of a novel mode splitter for multimode communication systems," in *Computers and Devices for Communication (CODEC), International Conference on*, pp. 1–4, IEEE, 2015.
24. S. L. Hada and B. M. A. Rahman, "Rigorous analysis of numerical methods: a comparative study," Opt. Quantum Electron. **48**(6), 309 (2016).
25. B. M. A. Rahman and J. B. Davies, "Vector–**H** finite element solution of GaAs/GaAlAs rib waveguides," IEE Proc. J. Optoelectron. **132**(6), 349–353 (1985).
26. B. M. A. Rahman and J. B. Davies, "Analysis of optical waveguide discontinuities," J. Lightwave Technol. **6**(1), 52–57 (1988).
27. P. Dong, W. Qian, H. Liang, R. Shafiiha, D. Feng, G. Li, J. E. Cunningham, A. V. Krishnamoorthy, and M. Asghari, "Thermally tunable silicon racetrack resonators with ultralow tuning power," Opt. Express **18**(19), 20298–20304 (2010).
28. C. Qiu, W. Gao, R. Soref, J. T. Robinson, and Q. Xu, "Reconfigurable electro-optical directed-logic circuit using carrier-depletion micro-ring resonators," Opt. Lett. **39**(24), 6767–6770 (2014).
29. J. Schrauwen, D. Van Thourhout, and R. Baets, "Trimming of silicon ring resonator by electron beam induced compaction and strain," Opt. Express **16**(6), 3738–3743 (2008).
30. Y. Shen, I. B. Divliansky, D. N. Basov, and S. Mookherjea, "Electric-field-driven nano-oxidation trimming of silicon microrings and interferometers," Opt. Lett. **36**(14), 2668–2670 (2011).
31. M. M. Milosevic, X. Chen, W. Cao, A. F. Runge, Y. Franz, C. G. Littlejohns, S. Mailis, A. C. Peacock, D. J. Thomson, and G. T. Reed, "Ion implantation in silicon for trimming the operating wavelength of ring resonators," IEEE J. Sel. Top. Quantum Electron. **24**(4), 1–7 (2018).
32. S. Grillanda, V. Raghunathan, V. Singh, F. Morichetti, J. Michel, L. Kimerling, A. Melloni, and A. Agarwal, "Post-fabrication trimming of athermal silicon waveguides," Opt. Lett. **38**(24), 5450–5453 (2013).
33. V. R. Almeida, Q. Xu, C. A. Barrios, and M. Lipson, "Guiding and confining light in void nanostructure," Opt. Lett. **29**(11), 1209–1211 (2004).
34. B. M. A. Rahman, T. Wongcharoen, and K. T. V. Grattan, "Finite element analysis of nonsynchronous directional couplers," Fiber Integr. Opt. **13**(3), 331–336 (1994).

138.40.68.73 {ts '2020-09-02 09:14:54'}